Journal of Science and Technology in Civil Engineering, HUCE, 2024, 18 (3): 102–113

FLEXURAL AND FRACTURE BEHAVIOR OF HIGH-PERFORMANCE CONCRETE USING NOTCH SPECIMEN

Kha-Ky Lam[a], Duy-Liem Nguyen[a,*], Tuan Manh Le[a], Ngoc-Thanh Tran[b]

[a]*Faculty of Civil Engineering, Ho Chi Minh City University of Technology and Education, 01 Vo Van Ngan street, Thu Duc city, Ho Chi Minh city, Vietnam*
[b]*Institute of Civil Engineering, Ho Chi Minh City University of Transport, 02 Vo Oanh street, Binh Thanh district, Ho Chi Minh city, Vietnam*

Article history:
Received 02/4/2024, Revised 04/9/2024, Accepted 17/9/2024

Abstract

This study investigated the mechanical properties of high-performance concrete using notched specimens. All flexural specimens had an identical geometry of 40×40×160 mm^3 with a span length of 120 mm. Four notch-to-depth ratios were as follows: 0 (N0 series), 0.125 (N1 series), 0.250 (N2 series), and 0.375 (N3 series), which were designed at the specimen bottom of midspan section. The investigation focused on the four parameters of high-performance concrete, including load carrying, deflection capacity, flexural strength, and the critical stress intensity factor. The results showed that the load-carrying and deflection capacities decrease with an increase in the notch-to-depth ratios. Furthermore, the flexural strength was ranked as follows: N0 series > N3 series > N2 series > N1 series, whereas ranking of the regarding critical stress intensity factor was opposite: N1 series > N2 series > N3 series.

Keywords: high-performance concrete; notched specimen; load-carrying capacity; notch-to-depth ratio; critical stress intensity factor.

https://doi.org/10.31814/stce.huce2024-18(3)-08

1. Introduction

Concrete is a widely used material in civil and military infrastructure because of its relatively low cost and easily formed into various shapes and sizes for structures. Nowadays, the quick growth in civil engineering leads to a high demand in developing new concrete types, which can highly resist to mechanical and environmental loads. High-performance concrete (HPC) is a promising construction material due to its better mechanical performance compared to normal concrete (NC) [1–3]. In detail, HPCs containing suitable reinforcing fibers can produce compressive strength > 90 MPa [4–7], tensile strength > 10 MPa [8–10], flexural strength > 20 MPa [11, 12]. In addition, HPCs containing suitable reinforcing fibers can improve the brittle nature of concrete, produce large ductility, high energy absorption capacity, and crack resistance [13–17].

Designing or analyzing a reinforced concrete (R.C) structure are often based on stress-strain behaviors of concrete and reinforcement forming the structure [18]. Besides, to predict crack propagation and failure behavior of the R.C structure, fracture mechanisms of the concrete have been focused to study [19, 20]. In fracture mechanics, crack propagation has been distinguished by three models of crack surface displacement, including Mode I (opening mode), Mode II (in-plane shear mode), and Mode III (tearing of the plane) [21]. And, notched specimens have been commonly employed to determine fracture parameters, which were quantitatively characterized crack resistant property of concrete under loading [22–24]. Chiaia et al. [22] investigated the notched specimen of steel fiber-reinforced concrete under three-point bending test. The authors reported that the relationship between

*Corresponding author. *E-mail address:* liemnd@hcmute.edu.vn (Nguyen, D.-L.)

crack mouth opening displacement (CMOD) and mid-span displacement did not depend on the fiber content. Jiao et al. [23] studied the effect of notch-to-depth (a/h) ratios of 0.2, 0.3, 0.4, and 0.5 on the flexural and fracture behaviors of ultra-high-performance glass sand concrete under a four-point bending test. The results showed that the increase in depth of notch led to reduction in peak load. Moreover, compared to a/h of 0.2, the flexural strength decreased by 14.77%, 16.08%, and 10.06% for a/h = 0.3, 0.4, and 0.5, respectively. Yin et al. [24] also observed that the load capacity of concrete decreased as the a/h of specimen increased from 0.2 to 0.6. In addition, the constant fracture toughness and the constant fracture energy of concrete were also derived.

Although there have been some published references about fracture behavior of high-performance concrete using notch specimens, the information on this matter is still limited and requires more further studies. The situation has motivated this study, which includes two main objectives as follows: (i) Evaluating flexural behavior of HPC with different notch depth specimens; (ii) Evaluating fracture behavior of HPC with different notch depth specimens. It is highly expected that the findings of this study work will provide helpful information on the flexural and fracture behavior of HPC, which partly contribute to widen practical application of HPC.

2. Typical flexural behavior of HPCs

2.1. Flexural behavior of HPC using notch specimen

Fig. 1 displays the typical applied load (P) versus deflection (δ) response of HPC. According to Fig. 1, the peak of the response curve provides load-carrying capacity (P_{MOR}) and deflection capacity (δ_{MOR}). With an absence of reinforcing fibers in HPC, the response beyond the peak load is usually brittle with a sudden drop in load [25], which indicates unstable crack propagation process. The flexural strength (f_{MOR}) of studied concrete was performed based on the standard TCVN 3121-11:2022 with three-point bending loading [26].

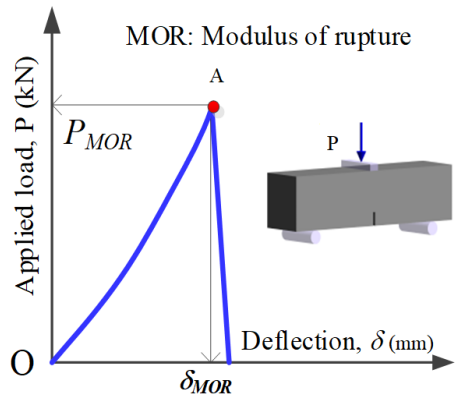

Figure 1. Typical load versus deflection response curve of HPCs

The moment (M_{MOR}) and flexural strength (f_{MOR}) of the notch specimens are determined according to Eqs. (1) and (2), respectively, as follows:

$$M_{MOR} = \frac{P_{MOR}L}{4} \tag{1}$$

$$f_{MOR} = \frac{3P_{MOR}L}{2b\,(h-a)^2} \tag{2}$$

In Eqs. (1) and (2), where P_{MOR}, L = 120 mm, b = 40 mm, h = 40 mm, and a = 0, 5, 10, 15 mm are the peak load, span length, width, depth, and notch depth of the specimen, respectively.

2.2. Fracture behavior of HPC using notch specimen

In fracture mechanics, Linear Elastic Fracture Mechanics (LEFM) refers to fracture happening at the nominal stress much lower than yield stress of a material. The primary assumption of LEFM is that wasted energy is a small area at the crack tip (small-scale yielding) and brittle fracture performs little or no plastic deformation. To quantitatively assess the resistance to crack propagation of the

material, critical stress intensity factor (K_{IC}) is often used as fracture strength\toughness, a material property. Fig. 2 presents the fracture behavior of brittle, ductile and quasi-brittle materials with their zone of cohesive softening fracture mechanics after crack tip [27]. As can be seen in Fig. 2, both zones of softening and nonlinear hardening fracture mechanics of brittle material are small. Fig. 3 displays the typical crack tip stress field under three-point bending in Mode I relating to stress intensity factor (K_I) of the material. The critical stress intensity factor in Mode I of HPC under three-point bending is computed by Eqs. (2) and (3):

$$K_{IC} = 6Y(\alpha) M_{MOR} \times \frac{\sqrt{a}}{bh^2} \tag{3}$$

$$Y(\alpha) = \frac{\left[1.99 - \alpha \times (1-\alpha)\left(2.15 - 3.93\alpha + 2.7\alpha^2\right)\right]}{(1+2\alpha)(1-\alpha)^{3/2}}; \quad 0 < \alpha = \frac{a}{h} < 1 \tag{4}$$

where K_{IC}, $Y(\alpha)$, and M_{MOR} are critical stress intensity factor, geometry factor, and moment at modulus of rupture, respectively; $\alpha = \frac{a}{h}$ is the notch-to-depth ratio, $\alpha = \frac{a}{h} = 0, 0.125, 0.250, 0.375$ in this study.

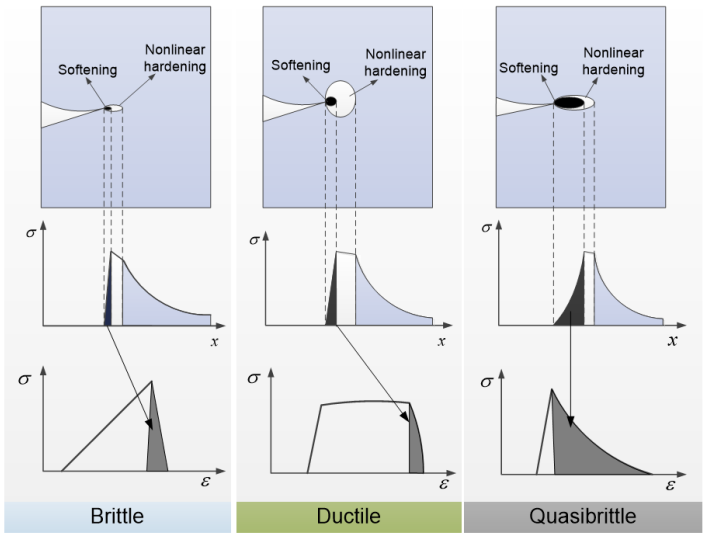

Figure 2. Fracture behavior of brittle, ductile and quasi-brittle materials

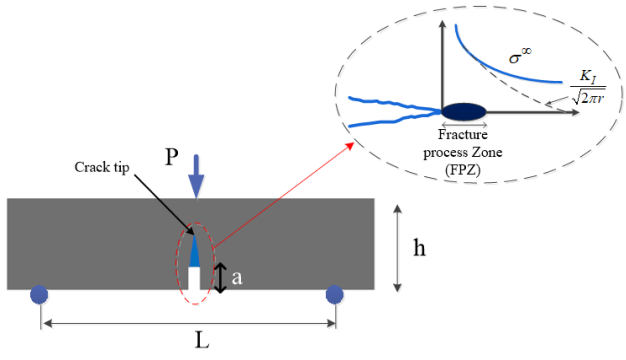

Figure 3. Typical crack tip stress field under three-point bending in Mode I

3. Experiment setup

3.1. Experimental program

Fig. 4 displays the experimental layout for exploring the flexural behavior of the HPC using notch specimens subjected to three-point bending. As can be seen from Fig. 4, four notch-to-depth ratios are investigated as follows: 0 (no notch, notation N0 series), 0.125 (notch depth of 5 mm, notation N1 series), 0.250 (notch depth of 10 mm, notation N2 series), and 0.375 (notch depth of 15 mm, notation N3 series), all the notches are at the specimen bottom of midspan section. The investigated parameters of the HPC using notch specimens are P_{MOR}, f_{MOR}, δ_{MOR}, and K_{IC}.

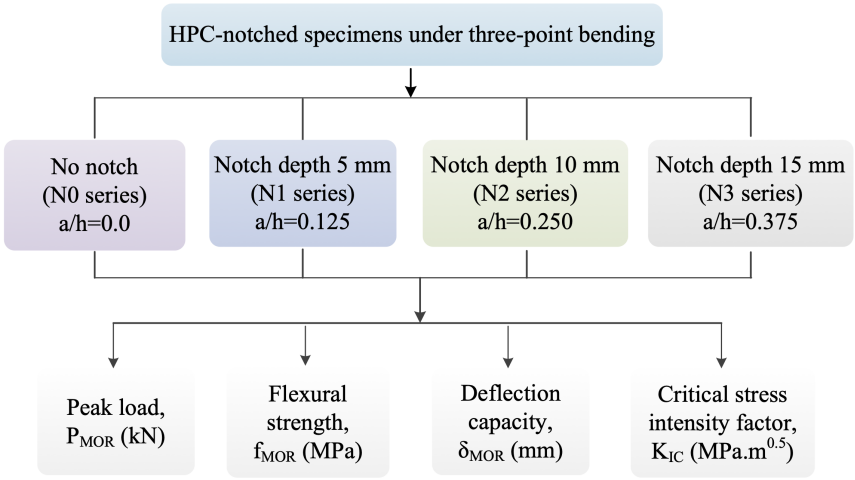

Figure 4. Layout of the experiment

3.2. Materials and experimental preparation

All the flexural specimens have a prism shape with a cross section of 40×40 mm^2 and a length of 160 mm (span length of 120 mm). Table 1 shows the composition of the HPC with a compressive strength of 79.6 MPa [28]. Fig. 5 shows the photos of the compositional materials used. Table 2 provides the chemical and physical properties of cement, fly ash, and silica fume, while Table 3 supplies the properties of silica sand and the superplasticizer.

Table 1. Composition and compressive strength of HPC

Mixture type	Weight ratio
Cement (Insee, PC40)	0.80
Silica Fume	0.07
Silica sand	1.00
Superplasticizer	0.04
Fly-ash	0.2
Water	0.26
Compressive strength (MPa)	79.6 [27]

The mixing of the HPC mixture was carried out in a laboratory with a temperature of 25 ± 50 °C and a humidity of 70 ± 5%. Firstly, the cement, silica sand, and fly ash were dry-mixed for about 10 minutes. Next, the water was added and mixed further for about 5–10 minutes. Then, the superplasticizer was slowly added to the mortar matrix. When the mortar had a suitable flow ability

Table 2. The chemical and physical properties of cement, fly ash, silica fume

Chemical and physical	Cement (Insee, PC 40)	Fly ash	Silica fume
SiO_2 (%)	20.60	56.25	95.38
CaO (%)	62.6	1.90	0.13
Al_2O_3 (%)	5.10	20.04	0.2
MgO (%)	3.00	1.30	0.37
Fe_2O_3 (%)	3.20	3.48	0.0063
SO_3 (%)	3.60	0.58	-
$K_2O + Na_2O$ (%)	1.40	1.02	1.81
C (%)	-	-	0.007
Loss on ignition (%)	0.30	9.52	3,859
Fineness (m^2/kg)	348	289	20,000
Specific gravity	3.15	2.41	2.24

Table 3. Properties of silica sand and superplasticizer used in this study

Properties	Silica sand	Superplasticizer
Name	-	Adva Cast 512 - W.R. Grace
Density (g/cm^3)	2.65	-
Chemical origin	-	Naphtalen Formadehyt Sulfonat
Maximum size of diameter (mm)	1.00	-
Volumetric mass (g/cm^3)	1.56	1.19 – 1.22

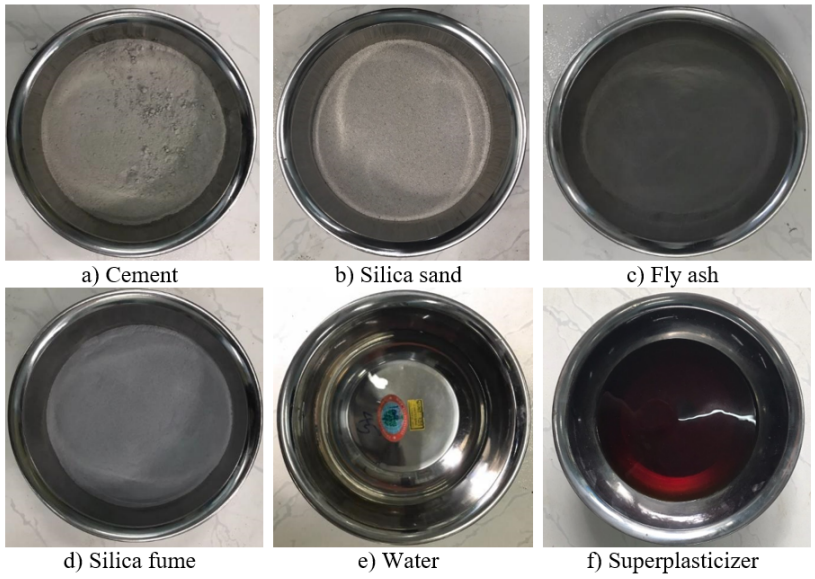

Figure 5. Photos of the compositional materials used to produce the HPC

for workability (the slump-flow values of 60-70 cm) [29], the mortar matrix was placed into the mold. The flexural specimens after casting were covered with a plastic sheet for 24 hours at room temperature. After demolding, the specimens were cured in water for 28 days at a temperature of 25 °C. Fig. 6 shows the geometry and preparation of the different-depth notched specimen. At the

middle span, the bottoms of the specimens were notched with various designed depths of 0, 5, 10, and 15 mm using a 2 mm-thick saw. At least three specimens from each series were examined.

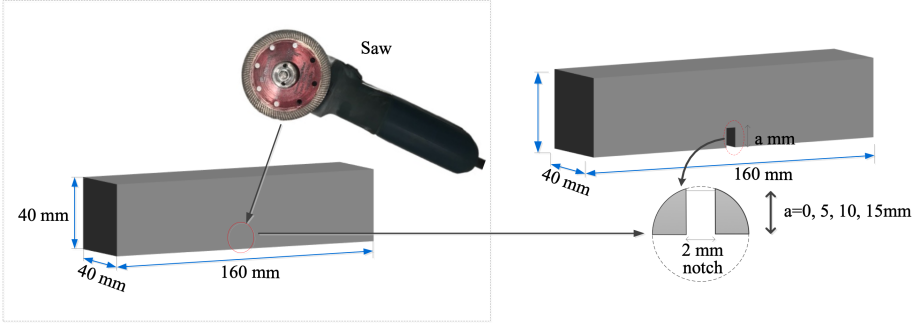

Figure 6. Geometry and preparation of different-depth notched specimens

3.3. Test setup

Fig. 7 shows the experimental set-up under three-point bend test, which is conducted using a dynamic testing system (DTS) with a load capacity of 30 kN. The applied load velocity is controlled at 1 mm/min. During the test, the data acquisition of load and deflection at the middle span were set at 1 Hz.

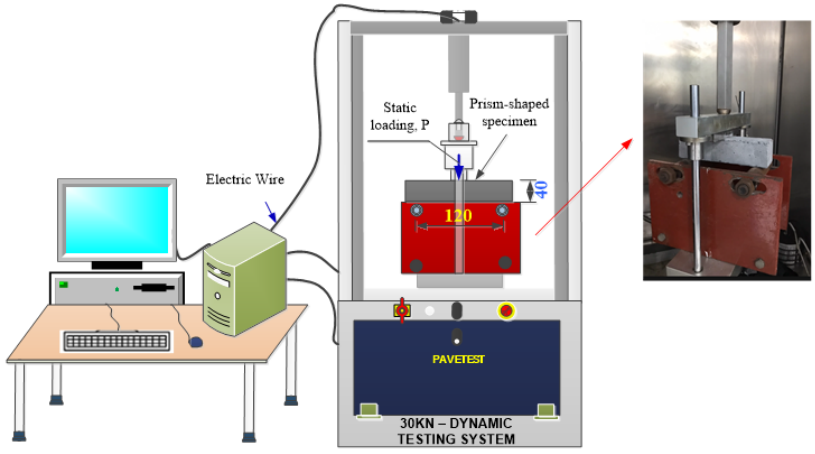

Figure 7. Experimental set-up under three-point bend test

4. Experiment result and discussion

4.1. Flexural behaviors of HPC

Fig. 8 displays the load-deflection responses of the HPC with different notch depths of the tested specimens. Table 4 provides three mechanical parameters of P_{MOR}, f_{MOR}, and δ_{MOR}. According to Table 4, the P_{MOR} varied from 4.47 to 1.72 kN, i.e., the f_{MOR} were from 10.31 to 12.58 MPa. The δ_{MOR} ranged from 0.34 to 0.50 mm corresponding to the P_{MOR}. Fig. 9 shows the comparisons of P_{MOR}, f_{MOR}, and δ_{MOR} regarding different notch depth specimens. Compared to the N0 series, the N1 series produced a decrement in P_{MOR} with 0.63 times, the N2 series with 0.48 times, and the N3 series with 0.38 times. The P_{MOR} and δ_{MOR} decreased as the notch depth of specimen increased. This observation can simply be attributed that the working section becomes weaker as the notch depth increases. However, the order of the HPC series in term of f_{MOR} was: N1 series < N2 series < N3 series

< N0 series, i.e., the f_{MOR} increased as the notch depth of specimen increased, excluding the case of no notch specimen. This tendency can be explained according to size effect law for brittle materials: the smaller specimen section results in the higher strength [30]. Besides, the flexural strength increases with an increase in the notch-to-depth ratios of this study, which also performed the same tendency with the study result of Jiao et al. [23] for notched specimens. It can be concluded that the tendency of flexural strength of notched HPFRC specimens in this study is rather usual.

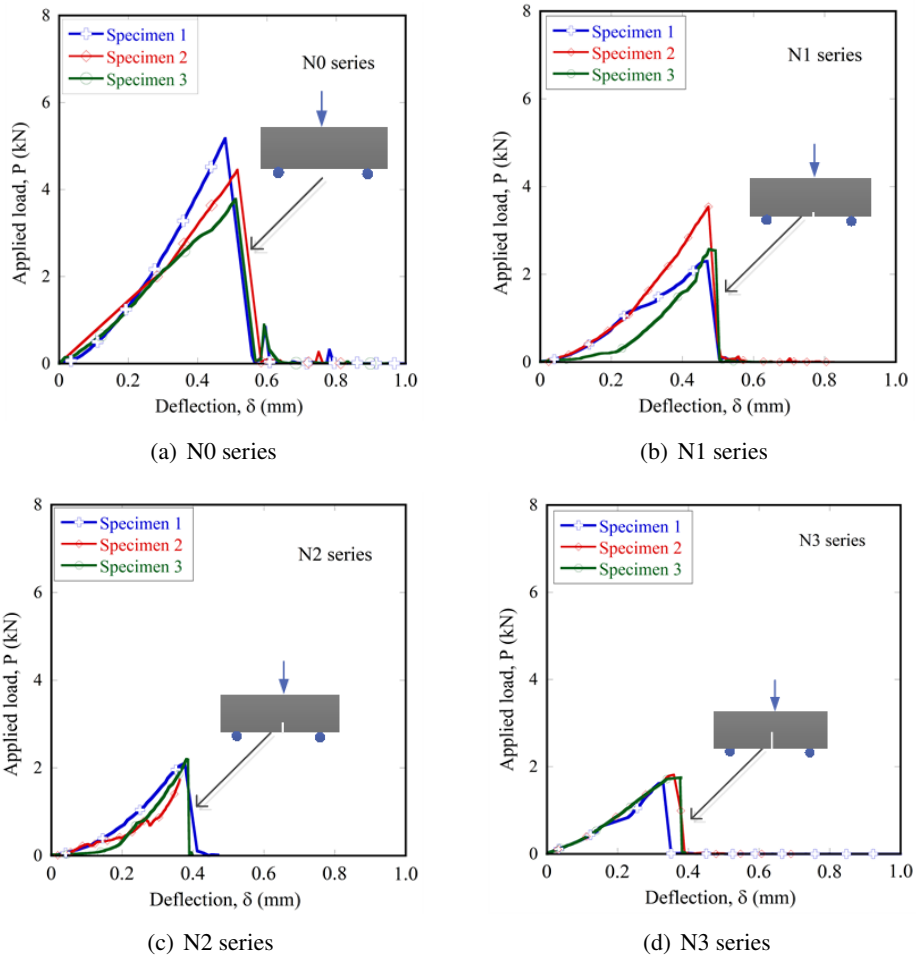

(a) N0 series (b) N1 series

(c) N2 series (d) N3 series

Figure 8. Load versus deflection behavior of the studied specimens

Table 4. Parameters of P_{MOR}, f_{MOR}, and δ_{MOR} regarding different notch-to-depth ratios

Test series	Specimen	Peak load, P_{MOR} (kN)	Deflection, δ_{MOR} (mm)	Flexural strength, f_{MOR} (MPa)
N0 series [27]	Spe. 1	5.18	0.48	14.56
	Spe. 2	4.46	0.51	12.54
	Spe. 3	3.78	0.51	10.63
Average value		**4.47**	**0.50**	**12.58**
(Standard deviation)		**(0.70)**	**(0.02)**	**(1.97)**

Test series	Specimen	Peak load, P_{MOR} (kN)	Deflection, δ_{MOR} (mm)	Flexural strength, f_{MOR} (MPa)
N1 series	Spe. 1	2.30	0.47	8.46
	Spe. 2	3.55	0.47	13.03
	Spe. 3	2.57	0.48	9.45
Average value		**2.81**	**0.47**	**10.31**
(Standard deviation)		**(0.80)**	**(0.09)**	**(2.60)**
N2 series	Spe. 1	2.11	0.38	10.53
	Spe. 2	2.14	0.38	10.69
	Spe. 3	2.20	0.38	11.01
Average value		**2.16**	**0.38**	**10.74**
(Standard deviation)		**(0.10)**	**(0.0005)**	**(0.49)**
N3 series	Spe. 1	1.63	0.30	11.75
	Spe. 2	1.82	0.34	13.08
	Spe. 3	1.72	0.38	12.41
Average value		**1.71**	**0.34**	**12.42**
(Standard deviation)		**(0.09)**	**(0.04)**	**(0.67)**

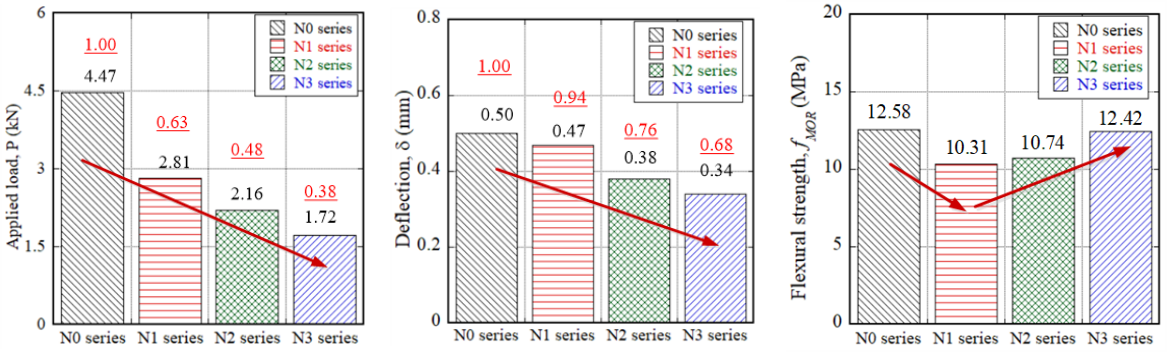

(a) P_{MOR} (b) δ_{MOR} (c) f_{MOR}

Figure 9. Comparisons of P_{MOR}, f_{MOR}, and δ_{MOR} regarding different notch-to-depth ratios

4.2. Critical stress intensity factor of HPC

Table 5 provides the K_{IC} values of different notch depth specimens. Based on the P_{MOR}, the corresponding M_{MOR} were obtained in range of 63.15-106.43 kN.mm, and the K_{IC} changed from 0.58 to 1.01 MPa.m$^{0.5}$. Fig. 10 displays the photos of cracking patterns of the specimens. Fig. 11 shows the comparisons of K_{IC} and their regression analysis according to notch-to-depth ratio. The K_{IC} and of the HPC decreased as the notch depth of specimen increased, not considering the case of no notch specimen. In addition, the K_{IC} of the HPC regarding notch-to-depth ratio was observed to be higher than that of normal concrete (NC) , examined by Dong et al. [31], despite their same tendency of K_{IC} as comparatively shown in Fig. 11(b). The regression analyses between $K_{IC}$and α of HPC and

NC as Eq. (5):

$$\begin{cases} K_{IC} = 3.41\alpha^2 - 3.41\alpha + 1.38 & \text{for HPC} \\ K_{IC} = 2.44\alpha^2 - 2.59\alpha + 1.15 & \text{for NC} \end{cases} \quad (5)$$

Table 5. Parameter of K_{IC} regarding different notch-to-depth ratios

Test series	Ratio of $\alpha = \frac{a}{h}$	Applied load, P_{MOR} (kN)	Maximum moment M_{MOR} (kN.mm)	Critical stress intensity factor K_{IC} (MPa.m$^{0.5}$)
N1 series (Notch 5 mm)	0.125	2.30 3.55 2.57	69.06 106.43 77.14	0.83 1.28 0.92
Average value Standard deviation)	-	**2.81** (0.66)	**84.21** (19.66)	**1.01** (0.24)
N2 series (Notch 10 mm)	0.250	2.11 2.14 2.20	63.15 64.16 66.07	0.73 0.74 0.76
Average value Standard deviation)	-	**2.15** (0.05)	**64.46** (1.48)	**0.74** (0.02)
N3 series (Notch 15 mm)	0.375	1.63 1.82 1.72	48.96 54.52 51.73	0.55 0.62 0.58
Average value Standard deviation)	-	**1.72** (0.09)	**51.74** (2.78)	**0.58** (0.03)

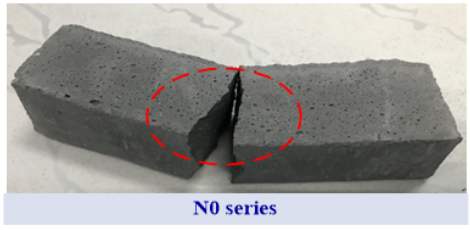

(a) No notch specimen

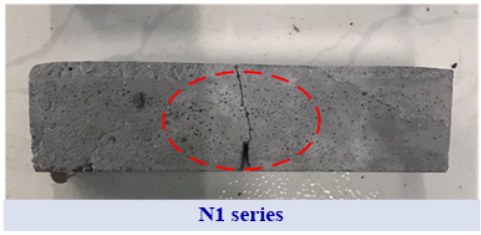

(b) 5 mm notch specimen

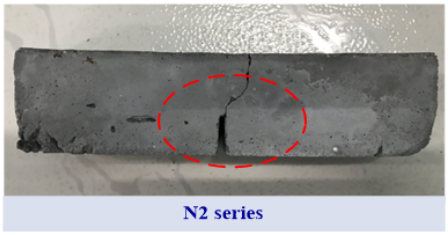

(c) 10 mm notch specimen

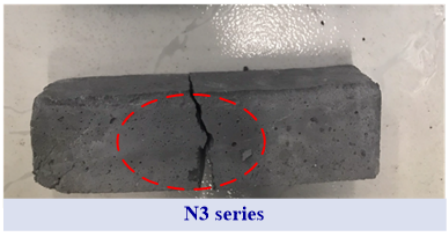

(d) 15 mm notch specimen

Figure 10. Photos of cracking behaviors according to different notch-to-depth ratios

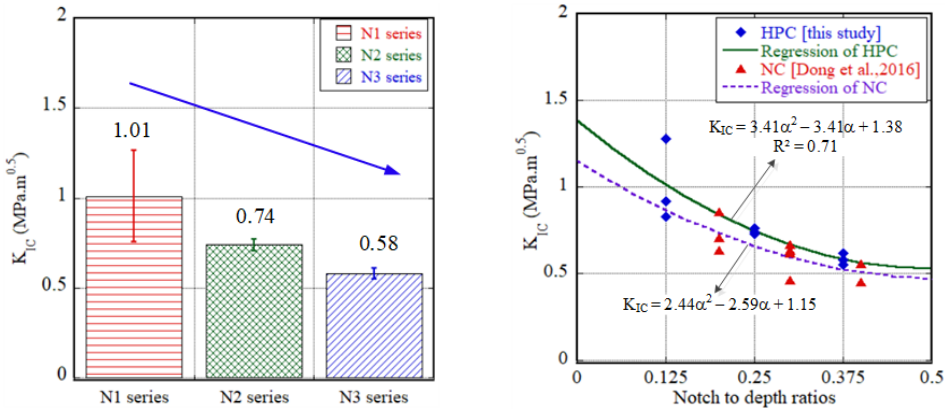

(a) K_{IC} of HPC (b) Regression analysis of K_{IC}

Figure 11. Performance of K_{IC} according to different notch-to-depth ratios

5. Conclusions

Based on the experimental and analysis results, some main conclusions can be drawn as follows:

- The load-carrying capacity and deflection capacity decreased with increase in notch-to-depth ratio of the flexural HPC.

- The flexural strength increased with increase in notch-to-depth ratio of the flexural HPC, excluding the case of no notch specimen.

- The flexural strength of no notch specimen was higher than notch specimen, regardless of notch depth of the HPC.

- The critical stress intensity of the HPC ranged from 0.58 to 1.01 MPa.m$^{0.5}$, it decreased with increase in notch-to-depth ratio of the flexural HPC. The trends between flexural strength and critical stress intensity were opposite with the increment in notch-to-depth ratio of the flexural HPC.

- The K_{IC} of the HPC regarding notch-to-depth ratio was observed to be relatively higher than that of normal concrete, although these concrete types demonstrated the same tendency as notch depth varied.

Acknowledgments

This research is funded by Vietnam National Foundation for Science and Technology Development (NAFOSTED) under grant number 107.01-2021.69.

References

[1] Naaman, A. E., Reinhardt, H. W. (1996). Characterization of high performance fiber reinforced cement composites. In *High Performance Fiber Reinforced Cement Composites*, volume 2, 1–24.

[2] Liem, N. D., Ngo, T.-T., Phan, T.-D., Lai, T.-T., Le, D.-V. (2022). Predicting tensile properties of strain-hardening concretes containing hybrid fibers from single fiber pullout resistance. *Journal of Science and Technology in Civil Engineering (JSTCE)-HUCE*, 16(3):84–96.

[3] Vatannia, S., Kearsley, E., Mostert, D. (2020). Development of economic, practical and green ultra-high performance fiber reinforced concrete verified by particle packing model. *Case Studies in Construction Materials*, 13:e00415.

[4] Shin, K.-J., Jang, K.-H., Choi, Y.-C., Lee, S.-C. (2015). Flexural behavior of HPFRCC members with inhomogeneous material properties. *Materials*, 8(4):1934–1950.

[5] Tran, T. K., Kim, D. J. (2014). High strain rate effects on direct tensile behavior of high performance fiber reinforced cementitious composites. *Cement and Concrete Composites*, 45:186–200.

[6] Wille, K., Kim, D. J., Naaman, A. E. (2011). Strain-hardening UHP-FRC with low fiber contents. *Materials and Structures*, 44:583–598.
[7] Zia, P. (1991). *High performance concretes: A state-of-the-art report*, volume 91. Strategic Highway Research Program, National Research Council.
[8] Park, S. H., Kim, D. J., Ryu, G. S., Koh, K. T. (2012). Tensile behavior of ultra high performance hybrid fiber reinforced concrete. *Cement and Concrete Composites*, 34(2):172–184.
[9] Nguyen, D.-L., Nguyen, T.-Q., Nguyen, H.-T.-T. (2020). Influence of fiber size on mechanical properties of strain-hardening fiber-reinforced concrete. *Journal of Science and Technology in Civil Engineering (JSTCE)-HUCE*, 14(3):84–95.
[10] Hai, H. V. (2023). Experimental and numerical study on tensile behavior of ultra high-performance concrete. *Transport and Communications Science Journal*, 74(6):709–717.
[11] Kim, D. J., Park, S. H., Ryu, G. S., Koh, K. T. (2011). Comparative flexural behavior of hybrid ultra high performance fiber reinforced concrete with different macro fibers. *Construction and Building Materials*, 25(11):4144–4155.
[12] Wang, D., Ju, Y., Shen, H., Xu, L. (2019). Mechanical properties of high performance concrete reinforced with basalt fiber and polypropylene fiber. *Construction and Building Materials*, 197:464–473.
[13] Kim, D. J., Wille, K., El-Tawil, S., Naaman, A. E. (2011). Testing of cementitious materials under high-strain-rate tensile loading using elastic strain energy. *Journal of Engineering Mechanics*, 137(4):268–275.
[14] Nguyen, D. L., Kim, D. J., Ryu, G. S., Koh, K. T. (2013). Size effect on flexural behavior of ultra-high-performance hybrid fiber-reinforced concrete. *Composites Part B: Engineering*, 45(1):1104–1116.
[15] Nguyen, D.-L., Thai, D.-K., Nguyen, H. T. T., Tran, N. T., Phan, T.-D., Kim, D. J. (2023). Mechanical behaviors and their correlations of ultra-high-performance fiber-reinforced concretes with various steel fiber types. *Structural Concrete*, 24(1):1179–1200.
[16] Nguyen, D.-L., Kim, D.-J., Thai, D.-K. (2019). Enhancing damage-sensing capacity of strain-hardening macro-steel fiber-reinforced concrete by adding low amount of discrete carbons. *Materials*, 12(6):938.
[17] Nguyen, D.-L., Ngo, T.-T., Tran, N.-T. (2021). Span length-dependent load-carrying capacity of normal concrete-HPFRC beams. *Journal of Science and Technology in Civil Engineering (JSTCE)-HUCE*, 15 (2):26–37.
[18] ACI 318-19 (2019). *Building code requirements for structural concrete*. American Concrete Institute, Farmington Hills, MI, USA.
[19] Clerc, G., Brunner, A. J., Niemz, P., van de Kuilen, J.-W. (2020). Application of fracture mechanics to engineering design of complex structures. *Procedia Structural Integrity*, 28:1761–1767.
[20] Accornero, F., Rubino, A., Carpinteri, A. (2022). A fracture mechanics approach to the design of hybrid-reinforced concrete beams. *Engineering Fracture Mechanics*, 275:108821.
[21] Shi, Z. (2009). *Crack analysis in structural concrete: theory and applications*. Butterworth-Heinemann.
[22] Chiaia, B., Fantilli, A. P., Vallini, P. (2007). Evaluation of minimum reinforcement ratio in FRC members and application to tunnel linings. *Materials and Structures*, 40:593–604.
[23] Jiao, Y., Fang, M., Han, X., Yang, H. (2023). Effect of notch-to-depth ratio on flexural and fracture behaviors of UHPGC notched beams based on four-point bending test and acoustic emission. *Engineering Fracture Mechanics*, 290:109524.
[24] Yin, Y., Qiao, Y., Hu, S. (2019). Four-point bending tests for the fracture properties of concrete. *Engineering Fracture Mechanics*, 211:371–381.
[25] Nguyen, D.-L., Lam, M. N.-T., Kim, D.-J., Song, J. (2020). Direct tensile self-sensing and fracture energy of steel-fiber-reinforced concretes. *Composites Part B: Engineering*, 183:107714.
[26] TCVN 3121-11:2022. *Mortar for masonry - Test methods - Part 11: Determination of flexural and compressive strength of hardened.*
[27] Bažant, Z. P. (2019). Design of quasibrittle materials and structures to optimize strength and scaling at probability tail: an apercu. *Proceedings of the Royal Society A*, 475(2224):20180617.
[28] Nguyen, T.-K., Nguyen, D.-L., Huy-Viet, L. E., Tran, N.-T. (2023). Fiber fraction-dependent flexural behavior of high-performance fiber-reinforced concrete under static and repeated loading. *Journal of Building Engineering*, 79:107808.

[29] Nguyen, D.-L., Nguyen, P.-C., Nguyen, V.-T., Luu, M. (2018). Comparative structural and non-structural properties of ultra high-performance steel-fiber-reinforced concretes and high-performance steel-fiber-reinforced concretes. In *2018 4th International Conference on Green Technology and Sustainable Development (GTSD)*, IEEE, 788–791.

[30] Weibull, W. (1951). A statistical distribution function of wide applicability. *Journal of Applied Mechanics*, 18:293–297.

[31] Dong, W., Wu, Z., Zhou, X., Wang, C. (2016). A comparative study on two stress intensity factor-based criteria for prediction of mode-I crack propagation in concrete. *Engineering Fracture Mechanics*, 158: 39–58.